

Synthesis and Characterization of Nano- crystalline Bixbyite-Hopcalite Solids

N. M. Deraz¹ and Omar H. Abd-Elkader²

¹Chemistry Department , College of Science, King Saud University, P.O. Box 2455, Riyadh 11451, Saudi Arabia.

²Electron Microscope Unit, Zoology Department, College of Science, King Saud University, Riyadh 11451, Kingdom of Saudi Arabia.

Received: 19 May 2013 / *Accepted:* 10 June 2013 / *Published:* 1 July 2013

Hopcalite based nano-materials were prepared by glycine assisted combustion method with different amounts of glycine. X-ray diffraction (XRD) and infrared (IR) measurements display the structural properties of hopcalite solid including the crystallite size, lattice constant, unit cell volume, X-ray density, the distance between the reacting ions, ionic radii, bond lengths on tetrahedral and octahedral sites involved in the spinel structure and ionic configuration of hopcalite studied.

Keywords: XRD; $\text{Cu}_{1.5}\text{Mn}_{1.5}\text{O}_4$, Cu-Mn- O system; hopcalite nano- particles.

1. INTRODUCTION

Spinel type materials have different applications ranging from optics, electronics, catalysis, magnetism, negative temperature coefficient (NTC) ceramic thermistors to conversion and energy storage [1, 2]. The cubic spinel structure, has a structural formula AB_2O_4 based on the cubic close packing of oxygen ions in which cations are situated on both tetrahedral (A sites) and octahedral (B sites) [3, 4]. Today, one of the important spinel ceramic materials is hopcalite depending upon low cost, ease of manufacturing and interesting catalytic and thermistor properties. Hopcalite is copper manganite, $\text{Cu}_x\text{Mn}_{3-x}\text{O}_4$, having a flexible valence in $\text{Cu}^{1+/2+}$ and $\text{Mn}^{3+/4+}$ giving rise to its particular properties [1]. Spinel copper mandanite, CuMn_2O_4 , is widely used as a material for negative temperature coefficient (NTC) thermistors [5, 6]. The mechanism responsible for conduction in copper manganite is phonon assisted electron jumping (hopping) between Mn^{3+} and Mn^{4+} cations occupying octahedral sites [7]. The Cu–Mn–O systems have environmental importance because they are potential candidates for many catalytic reactions [8, 9]. Indeed, Cu–Mn mixed oxides in the form of hopcalite,

CuMn_2O_4 , have been used for ambient CO oxidation, especially in mining industries [10, 11]. Hopcalite is a well known oxidation catalyst to remove air pollutants such as carbon monoxide and nitrous oxide from exhaust gas [12]. Recently, this catalyst has been applied in the catalytic steam reforming of methanol [13].

Carus Corporation is the manufacturer of a series of manganese based catalysts, called CARULITE® catalysts. Hopcalite (also searched as Hopkalite) type catalysts are used for breathable air purification, emission air purification, and process air purification [14]. This corporation referred that [14]: (i) the mentioned catalysts can be used as materials for removal of deadly carbon monoxide from compressed breathing air sources. It also provides for removal of carbon monoxide in respirators/escape masks, as well as in the production of some gases with a high purity such as nitrogen, oxygen and argon. (ii) Using of hopcalite based materials led to effectively destroy for ozone emitted from various off-gas emissions, converting toxic ozone to oxygen. (iii) These materials brought about an effectively destroy for the volatile organic compounds (VOC) such as flexographic and rotogravure solvents, at temperatures considerably lower than those required for precious metal catalysts. The major sources of VOCs are the paint industry, building materials, automobile exhaust, combustion exhaust, industrial off gases, personal care products as well as a range of other sources [15]. (iv) Cu- Mn- O system is used to effectively destroy ethylene oxide emissions resulting from sterilization of medical equipment and supplies. In addition, the catalyst converts toxic ethylene oxide at low temperatures to carbon dioxide and water.

In fact, there are different hypotheses about the exact phase responsible for the high catalytic activity in Cu-Mn mixed oxides. One hypothesis is that the high activity is due to the formation of spinel CuMn_2O_4 solid depending upon the redox reaction $\text{Cu}^{2+} + \text{Mn}^{3+} = \text{Cu}^{1+} + \text{Mn}^{4+}$ yielding an electronic transfer between copper and manganese cations within the spinel lattice [16]. Another hypothesis attributes the high oxidation activity at room temperature to the so called ‘amorphous’ copper manganese oxide instead of the spinel CuMn_2O_4 [17]. In other words, this speculation refers to formation of a mixture of ultra fine particles with very small sizes of both copper and manganese oxide. In this case, Cu-Mn mixed oxides have high surface area with subsequent increase in the contact surface area involved in the catalytic reactions

Thermal decomposition of various precursors of different transition metals such as hydroxides, carbonates, nitrates and oxalates resulted in formation of numerous mixed oxides. Numerous routes have been used to synthesize Cu-Mn-O system including co-precipitation, high temperature ceramic method, sol-gel, redox-precipitation, soft reactive grinding, synthesis under supercritical water conditions, reverse micro-emulsion and the combustion method [18- 24]. Recently, my research group reported a novel method for synthesis of single oxides using glycine assisted combustion method nano-scale oxide dispersion [25]. This method is an effective strategy to obtain morphology-controllable materials with structural specificity, complexity, and related unique functions [26, 27]. This investigation demonstrates for the first time experimental method for the preparation of nanocrystalline manganite spinel by controlling in the ratio between the amounts of glycine and metal nitrates.

This study is devoted to the synthesis of copper manganite (hopcalite) by combustion synthesis. Another aim of this research is to obtain more information about effects of both glycine content and

calcination temperature on the formation and structural properties of hopcalite nano-particles. XRD technique is used for determining the structural properties of the final products.

2. EXPERIMENTAL

2.1. Preparation of nano- materials

Two samples of Cu/Mn mixed oxides were prepared by mixing calculated amounts of copper and manganese nitrates with different proportions of glycine [25]. The mixed precursors were concentrated in a porcelain crucible on a hot plate at 350 °C for quarter hour. The crystal water was gradually vaporized during heating and when a crucible temperature was reached, a great deal of foams produced and spark appeared at one corner which spread through the mass, yielding a voluminous and fluffy product in the container. In this investigation, the ratio of the glycine: copper: manganese nitrates were (0 and 4): 1: 2 for S1 and S2 samples, respectively. An additional sample, S3, was prepared by heating a part from the S2 sample at 900 °C for 2h. The chemicals employed in the present work were of analytical grade supplied by Prolabo Company. A general flowchart of the synthesis process is shown in Fig. 1.

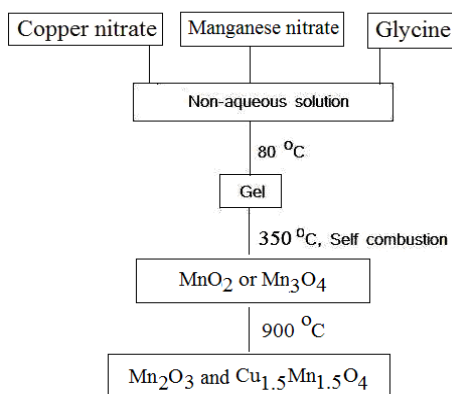


Figure 1. Process flowchart for fabricating the as prepared samples.

2.2. Characterization technique

An X-ray measurement of various mixed solids was carried out using a BRUKER D8 advance diffractometer (Germany). The patterns were run with Cu K_{α} radiation at 40 kV and 40 mA with scanning speed in 2θ of $2^{\circ} \text{min}^{-1}$.

The crystallite size of $\text{Cu}_{1.5}\text{Mn}_{1.5}\text{O}_4$ present in the investigated solids was based on X-ray diffraction line broadening and calculated by using Scherrer equation [28].

$$d = \frac{B\lambda}{\beta \cos \theta} \quad (1)$$

where d is the average crystallite size of the phase under investigation, B is the Scherrer constant (0.89), λ is the wave length of X-ray beam used, β is the full-width half maximum (FWHM) of diffraction and θ is the Bragg's angle.

3. RESULTS

3.1. XRD study

The XRD pattern for S1, S2 and S3 samples are given in Fig. 2.

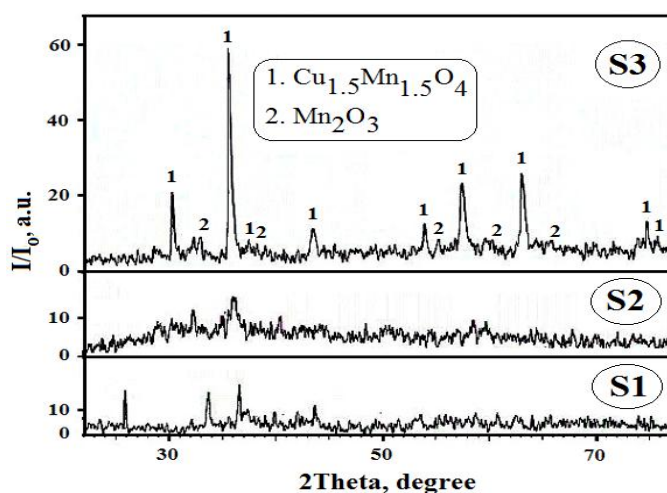


Figure 1. XRD pattern for the S1, S2 and S3 samples.

Inspection of this figure showed the following: (i) The S1 sample showed all the diffraction peaks of MnO_2 (pyrolusite and/or gamma phase) as a single phase (JCPDS card No. 12- 0715). The crystallinity of this phase is low indicating the formation of moderate crystalline MnO_2 particles with small crystallite size. (ii) The presence of small amount of glycine during the preparation process led to complete conversion of MnO_2 phase to Mn_3O_4 (hausmannite, JCPDS card No. 24- 0734) phase as shown in the S2 sample. The absence of copper oxide phase from the XRD patterns of samples S1 and S2 could be attributed to formation of solid solution between of Cu and Mn oxides and/or to formation of amorphous copper oxide phase. (iii) The S3 sample consisted entirely of both $\text{Cu}_{1.5}\text{Mn}_{1.5}\text{O}_4$ (Hopcalite, Major phase) and Mn_2O_3 (bixbyite, Minor phase). In other words, heating of the S2 sample at 900°C for 2h, as shown in S3 sample, led to complete conversion of Mn_3O_4 containing amorphous CuO to both $\text{Cu}_{1.5}\text{Mn}_{1.5}\text{O}_4$ and Mn_2O_3 phases (JCPDS card No. 70- 0260 and 70-0150, respectively). Indeed, $\text{Cu}_{1.5}\text{Mn}_{1.5}\text{O}_4$ phase involved in the S3 sample has cubic spinel structure with different planes (2 2 0), (3 1 1), (2 2 2), (4 0 0), (4 2 2), (3 3 3), (4 4 0) and (5 3 3). The space group of $\text{Cu}_{1.5}\text{Mn}_{1.5}\text{O}_4$ is $Fd3m$ (JCPDS card No. 70- 0260). The computed values of the crystallite size (d), lattice constant (a),

unit cell volume (V) and X-ray density (D_x) of $\text{Cu}_{1.5}\text{Mn}_{1.5}\text{O}_4$ phase, depending upon the data of X-ray, are given in Table 1.

Table 1. Crystallite size and lattice parameters $\text{Cu}_{1.5}\text{Mn}_{1.5}\text{O}_4$ phase.

Sample	$\text{Cu}_{1.5}\text{Mn}_{1.5}\text{O}_4$			
	d (nm)	a (nm)	V (nm^3)	D_x (g/cm^3)
S3	45	0.8270	0.5656	5.6754

From the data of X-ray, the distance between the reacting ions (L_A and L_B), ionic radii (r_A , r_B) and bond lengths (A–O and B–O) on tetrahedral (A) sites and octahedral (B) sites MgFe_2O_4 crystallites were summarized in Table 2.

Table 2. The values of L_A , L_B , A–O, B–O, r_A and r_B for $\text{Cu}_{1.5}\text{Mn}_{1.5}\text{O}_4$ phase.

Sample	L_A (nm)	L_B (nm)	A–O (nm)	B–O (nm)	r_A (nm)	r_B (nm)
S3	0.3581	0.2924	0.2005	0.0655	0.1943	0.05934

3.2. IR study

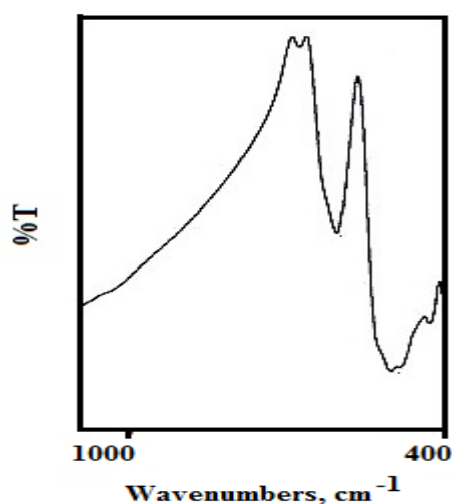


Figure 3. IR spectrum of the S3 sample.

The IR transmission spectrum for the S3 sample was recorded in the range of 1000- 400 cm^{-1} and is shown in Fig. 3. This figure showed two bands, ν_1 and ν_2 , at 601 and 498 cm^{-1} , respectively.

However, two shoulders around ν_1 and ν_2 bands at 750 cm^{-1} and 450 cm^{-1} . From IR data, the speculated configuration has been determined.

4. DISCUSSION

4.1. Formation of MnO_2 crystallites

Preliminary experiments showed formation of well crystalline CuO (Tenorite) by heating of copper nitrate on hotplate at $350\text{ }^\circ\text{C}$ for 15min. However, this treatment led to formation of a mixture of MnO_2 (pyrolusite and/or gamma phase as a major phase) and Mn_2O_3 (bixbyite). In other words, the relative abundance of MnO_2 was more pronounced compared to that of Mn_2O_3 [29]. In this study, the previous treatment of a mixture of copper and manganese nitrates resulted in formation of moderate crystalline of MnO_2 as a single phase. This indicates that the presence of copper hinders the transformation of MnO_2 phase to Mn_2O_3 phase.

4.2. Formation of Mn_3O_4 crystallites

In fact, the heat treatment of Mn_2O_3 phase at elevated temperatures, ranged between 800 and $900\text{ }^\circ\text{C}$, was normally accompanied by partial conversion into Mn_3O_4 (hausmannite) phase [30] according to the following reaction:



In this research, the thermal treatment for mixture of calculated amounts of glycine and Cu/Mn nitrates on the hotplate at $350\text{ }^\circ\text{C}$ brought about formation of a moderate crystalline Mn_3O_4 phase. This result indicated that the presence of the glycine as fuel led to the complete conversion of MnO_2 phase to Mn_3O_4 phase. These observations suggested that the MnO_x deposits coexist in intimate contact with CuO crystallites, favoring oxygen transfer between the two metal oxides. This type of MnO_2 -CuO structure interaction led to formation of the Mn_3O_4 phase. This indicated that there are existed a synergistic mechanism between the manganese and copper oxides. The proposed mechanism in this case is as follows:



It is well known that Cu_2O can be easily re-oxidized to CuO by exposure to air. Consequently, the suggested formation of Mn_3O_4 phase via the complete conversion of MnO_2 phase is according to the following reaction:



This observation shows the role of glycine as fuel in the promotion of moderate crystalline Mn_3O_4 particles.

4.3. Formation of spinel $\text{Cu}_{1.5}\text{Mn}_{1.5}\text{O}_4$ crystallites

Copper manganite can be prepared by ceramic route via solid state reaction between copper and manganese oxides [19]. The important factor that controls in the propagation of this reaction is the thermal diffusion of Cu and Mn cations through the thin manganite film which covers the surfaces of grains of reacting oxides containing Cu and Mn cations. This film acts as energy barrier to prevent the formation of excess amounts of manganite. Indeed, the control in this diffusion can be achieved by different factors such as doping, the degree of heat treatment, prolonged time of heat treatment and preparation route [25- 27]. The proposed mechanism of formation of copper manganite is according to the following stoichiometric reaction:



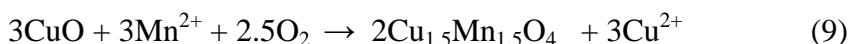
X-ray diffraction (XRD) studies of $\text{Cu}_x\text{Mn}_{3-x}\text{O}_4$ compound revealed the "normal" cubic spinel structure at room temperature [31]. It was later reported that pure cubic spinel CuMn_2O_4 could not be prepared at all [32–34]. In fact, it was shown that the S3 sample quenched at 900 °C resulted in cubic spinel $\text{Cu}_{1.5}\text{Mn}_{1.5}\text{O}_4$ phase with trace amount of $\gamma\text{-Mn}_2\text{O}_3$ as a secondary phase [35]. Similar results carried out the neutron diffraction experiments on quenched CuMn_2O_4 material reported to formation of $\text{Cu}_{1.5}\text{Mn}_{1.5}\text{O}_4$ phase with partial inverse spinel structure [33]. These observations were established that the only way in which an undistorted (cubic) spinel of the Cu–Mn–O system could be prepared was in non-stoichiometric, $\text{Cu}_{1.5}\text{Mn}_{1.5}\text{O}_4$, form. This depends upon the preparation method and condition of the thermal treatment.

The counter-diffusion of Cu^{2+} and Mn^{3+} through a relatively rigid manganite film led to the formation of $\text{Cu}_{1.5}\text{Mn}_{1.5}\text{O}_4$ particles. We speculate that the diffusing ions might be Mn^{3+} including Mn^{2+} . In addition, the following reactions indicate that $3\text{Mn}_2\text{O}_3$ decomposes to 3Mn^{2+} and oxygen gas at Mn_2O_3 - interface. Moreover, oxygen moves through the reacted area to be added to the CuO interface and form spinel by reacting with manganese ions:

At Mn_2O_3 interface:



At CuO interface:



4.4. Ionic configuration of copper manganite

The vibration of ions in the crystal lattice of solid can be determined by IR technique. Spinel based materials have two main metal- oxygen bands in IR pattern [36]. These bands display the tetrahedral (A-sites) and octahedral (B-sites) involved in the spinel structure according to the geometrical configuration of materials. The highest band ν_1 , generally observed around 600 cm^{-1} , corresponds to intrinsic stretching vibrations of metal at the tetrahedral site, whereas the ν_2 lowest band, usually observed around 400 cm^{-1} , is assigned to octahedral- metal stretching. In inverse manganite such as copper manganite, the ν_1 and ν_2 bands are due to $\text{Mn}^{3+}\text{-O}^{2-}$ complexes present at A- and B-sites. The Cu^{2+} ions occupy mainly the octahedral sites and fraction goes into tetrahedral sites as Cu^+ ions [37]. This would explain the existence of two weak shoulders around ν_1 and ν_2 bands as

shown in Fig. 3. IR spectra of the S3 consisted of ν_1 and ν_2 at 601 and 498 cm^{-1} , respectively. The first shoulder around ν_1 band has a value of 750 cm^{-1} relative to the presence of Cu^+ ions in A- site. However, the The first shoulder around ν_2 band has a value of 450 cm^{-1} relative to the presence of Cu^{2+} ions in B- site. On the basis of the above data and also on earlier studies, the inverted spinel structure can be assigned in the S3 sample having the formula $\text{Cu}_x\text{Mn}_{3-x}\text{O}_4$ [38, 39]. In this investigation, the speculated ionic configuration of copper manganite is similar to that suggested by Broemme and Brabers [38]. Indeed, the rate of reduction of both Mn^{3+} and Cu^{2+} i. e. the formation of fractions of Mn^{2+} and Cu^+ depends on the technologies of synthesis and the subsequent temperature treatment [37]. Various authors reported that Cu^+ can be formed during the sintering process of Cu - containing materials. They proved that Cu^+ ion prefers tetrahedral sites; however, any oxidation of Cu^+ to Cu^{2+} by cooling in air does not incorporation of the residual CuO into the spinel phase [40]. Opposite behavior was observed in the case of the S3 sample. This behavior resulted in formation of Cu-Mn-O system with copper-rich composition having the formula $\text{Cu}_{1.5}\text{Mn}_{1.5}\text{O}_4$. Indeed, XRD measurements showed that the S3 sample consisted of both $\text{Cu}_{1.5}\text{Mn}_{1.5}\text{O}_4$ as a major phase and Mn_2O_3 as a minor phase.

5. CONCLUSIONS

The main conclusions that may be derived from this study are:

1. Solid state reaction between Cu and Mn oxides resulted in formation copper manganite. XRD results showed that the heat treatment of a mixture containing the precursors of Cu and Mn brought about formation of MnO_2 phase. This treatment resulted in formation of Mn_3O_4 phase in presence of small amount of glycine as a fuel. The last treatment followed by heating at 900 °C led to formation of non- stoichiometric spinel copper manganite.

2. Bixbyite (Mn_2O_3) - hopcalite ($\text{Cu}_{1.5}\text{Mn}_{1.5}\text{O}_4$) nano- composite can be prepared via glycine-assisted combustion followed by heating at 900 °C for 2h. The major phase in this composite is $\text{Cu}_{1.5}\text{Mn}_{1.5}\text{O}_4$.

3. The hopcalite was prepared in nano-scale form with partial inverse spinel structure.

4. Different structural properties of $\text{Cu}_{1.5}\text{Mn}_{1.5}\text{O}_4$ solid were determined.

5. The geometric configuration of $\text{Cu}_{1.5}\text{Mn}_{1.5}\text{O}_4$ has been discussed.

ACKNOWLEDGEMENT

This project was supported by King Saud University, Deanship of Scientific Research, College of Science Research Centre.

References

1. Siham Behar, Philippe Gonzalez, Pierre Agulhon, Françoise Quignard, Dariusz S'wierczyn'ski, *Catal. Today* 189 (2012) 35
2. R.K. Kamat, G.M. Naik, *Sensor Rev.* 22(2002)334.
3. C. Zhao, B. Wang, P. Yang, L. Winnubst, C. Chen, *J. Eur. Ceram. Soc.* 28 (2008)35.

4. R. Kambale, N. Adhate, B. Chougule, Y. Kolekar, *J. Alloys Compd.* 491 (2010) 372.
5. K. Park, J. Lee, S. Kim, W. Seo, W. Cho, C. Lee, S. Nahm, *J. Alloys Compd.* 467(2009) 310–316.
6. S.A. Kanade, V. Puri, *J. Alloys Compd.* 475 (2009) 352–355.
7. K. Park, J. Lee, *J. Alloys Compd.* 475 (2009) 513–517.
8. M.R. Morales, B.P. Barbero, L.E. Cadus, *Fuel* 87 (2008) 1177.
9. M. Zimowska, Z.A. Michalik, R. Janik, T. Machej, J. Gurgul, R. P. Socha, J. Podobinski, E.M. Serwicka, *Catal. Today* 119 (2007) 321.
10. Q. Liang, X. Wu, D. Weng, H. Xu, *Catal. Today* 139 (2008) 113.
11. X. Du, Z. Yuan, L. Cao, C. Zhang, S. Wang, *Fuel Process. Technol.* 89(2008)131.
12. F. C. Buciuman, F. Patcas, T. Hahn, *Chem. Eng. Proc.* 38(1999)563.
13. J. Papavasiliou, G. Avgouropoulos, T. Ioannides, *J. Catal.* 251(2007)7.
14. <http://www.caruscorporation.com/content.cfm/catalysts>.
15. E. Noordally, J.R. Richmond, S.F. Tahir, *Catal. Today* 17 (1993) 359.
16. G. Fortunato, H.R. Oswald, A. Reller, *J. Mater. Chem.* 11 (2001) 905.
17. M. Kramer, T. Schmidt, K. Stowe, W.F. Maier, *Appl. Catal. A* 302 (2006)257.
18. E.C. Njagi, C.H. Chen, H. Genuino, H. Galindo, H. Huang, S.L. Suib, *Appl. Catal. B* 99 (2010) 103.
19. Y.I. Hasegawa, R.U. Maki, M. Sano, T. Miyake, *Appl. Catal. A* 371 (2009)67.
20. Y. Hasegawa, K. Fukumoto, T. Ishima, H. Yamamoto, M. Sano, T. Miyake, *Appl. Catal. B* 89 (2009) 420.
21. G.J. Hutchings, A.A. Mirzaei, R.W. Joyner, M.R.H. Siddiqui, S.H. Taylor, *Appl. Catal. A* 166 (1998) 143.
22. Q. Liu, L.C. Wang, M. Chen, Y.M. Liu, Y. Cao, H.Y. He, K.N. Fan, *Catal. Lett.* 121(2008)144.
23. D. Rangappa, S. Ohara, M. Umetsu, T. Naka, T. Adschiri, *J. Supercritical Fluids* 44 (2008) 441.
24. J. Papavasiliou, G. Avgouropoulos, T. Ioannides, *Appl. Catal. B* 66 (2006)168.
25. N.M. Deraz, A. Alarifi, *J. Analyt. Appl. Pyrolysis* 97 (2012) 55.
26. N. M. Deraz, Moustafa M. G. Fouda, *Int. J. Electrochem. Sci.* 8(2013) 2682.
27. N. M. Deraz, Moustafa M. G. Fouda, Synthesis, *Int. J. Electrochem. Sci.* 8(2013) 2756.
28. B.D. Cullity, Elements of X-ray Diffraction, Addison-Wesly Publishing Co. Inc. 1976 (Chapter 14).
29. R. Craciun, *Catal. Lett.* 55(1998) 25.
30. N. M. Deraz, M. A. El-Sayed, A. Abdel-Aal, *Adsorp. Sci. Technol.* 19(2001)541.
31. A.P.B. Shina, N.R. Sanjana, A.B. Biswas, *J. Phys. Chem.* 62 (1958) 191.
32. G. Blasse, *J. Phys. Chem. Solids* 27 (1966) 383.
33. R. Buhl, *J. Phys. Chem. Solids* 30 (1969) 805.
34. G.G. Robbrecht, C.M. Henriët-Iserentant, *Phys. Status Solidi* 41 (1970) K43.
35. R.E. Vandenberghe, G.G. Robbrecht, V.A.M. Brabers, *Mat. Res. Bull.* 8(1973) 571.
36. R. D. Waldron, *Phys. Rev.*99 (1955) 1727.
37. E. Kester, B. Gillot, C. Villette, Ph. Tailhades, A. Rousset, *Thermodynam. Acta*, 297 (1997) 71.
38. A.D.D. Broemme, V.A.M. Brabers, *Solid State Ionics* 16 (1985) 171.
39. N.M. Deraz, *J. Anal. Appl. Pyrolysis* 82 (2008) 212.
40. A. Bielanski, K. Dyrek, Z. Kluz, J. Slozynski, T. Tombiasz, *Bull. Acad. Pol. Sci.* 9 (1964) 657.